Full Length Research Paper

Numerical simulation of aerodynamic and thermal fields inside a cylinder of an alternative engine

Z. Barbouchi and J. Bessrour

Unité de recherche mécanique appliquée, ingénierie et industrialisation, Ecole nationale d'ingénieurs de Tunis- BP 37, 1002 Tunis Belvédère.

We are interested in the study of turbulent and instationary flow inside a cylinder of an alternative engine. The finite element method is used to solve equations model. As the domain of the flow is changing with time due to the moving piston, an arbitrary Lagrange eulerian technique is chosen to reply to this problem. The modelisation is based on classic k- ε model. In this paper, we will present instantaneous velocity, streamlines and temperature maps obtained at various crank angles. We validate our results with other numerical predictions.

Key words: Aerodynamic, turbulence, simulation, finite elements, arbitrary Lagrangian Eulerian, alternative engine.

INTRODUCTION

The identification of the aerodynamic and thermal fields inside a cylinder of alternative engine with internal combustion during the intake stroke is an important stage for the comprehension of physical phenomenon which occurs in the motor cycle. The movement of the inlet air in the cylinder has a great influence in to the performance of the engine. It governs directly the rate of filling up, the thermal exchanges and the combustion quality. It is well known that the structure of the turbulent flow field is a determining factor in the initiation, the rate of propagation and the efficiency of the combustion process in an internal combustion engine. The process of air admission is an instationary and complex phenomenon in a domain with variable geometry (the piston and the valve movements). Its study needs the coupling between the admission pipe and the cylinder to emphasize the flow structure in the valve zone characterized by geometric dimensions inferior to the pipe diameter and variable in time. The aerodynamic phenomena which take place at the level of the valves have been studied often through the experiments. Many experimental essays have been carried out in the case of stationary flows to characterize the air movement through the valves (Arcoumanis and

Bicen, 1982; Kang and Reitz, 1999; Snauwaert and Sierens, 1986; Tippelmann, 1977) and recently (Gazeaux and Thomas, 2001 ; Yun, 2002). It was established that the air flow through the valve interacts with the cylinder walls to create large swirling structures. Generally, the principal air movements were filed into categories: the rotary movement induced tangentially in the cylinder (swirl) and the rotary movement in the axial plane (tumble) (Heywood, 1987). It's clear that the flow generation with intense vorticity (swirl and/or tumble) in the cylinder during the intake stroke is an efficient tool to obtain a great intensity of turbulence which can be maintained during the compression stroke. The stability of these swirling movements allows so to maintain a large turbulence during the fuel injection phase and induce optimal conditions for the initiation and the development of the combustion process. The shape of the combustion chamber plays too an important role as for of the established flows.

The experimental characterisation of the flows inside a mono cylinder has interested many manufacturers through certain techniques of visualisation and the use of transparent cylinders (Ekchian and Hoult,1979; Hirotimi and Nagayama, 1981; Arcoumanis et al.,1982; Liou and Saltavicca 1985; Nadarajah and Balabani, 1998). The insufficiency of the measurement tools has often made difficult the detailed study of the flow process evolution.

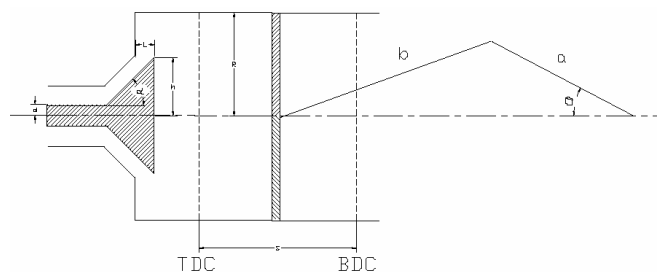*Corresponding author. E-mail: zouhaierbarbouchi@yahoo.fr.

Figure 1. Axisymmetric piston cylinder. R = 43.5 mm; h = 17 mm; d = 6.12 mm; α = 45°; S = 94 mm; L = 7.3 mm; a = stroke / 2; b = 363.5 mm.

Recently, the development of techniques based on velocimetry by means of particle images (PIV) has motivated manufacturers to study the evolution in time of the flow structure in the cylinder (Raffer and Willert,1998; Adrian, 1991; Khalighi, 1991; Lee and Farrel, 1993; Valentino 1993); Rouland and Floch, 1998).

A recent study (Huang, 2005) has allowed identifying the nature of the instantaneous flows during the intake and compression phases of a mono cylinder with two valves by means of two dimensions PIV technique.

The second approach, based on numerical modelisation and simulation of complex flows, has interested many authors for two decades. The majority have tried to bypass the numerical difficulties through some simplified hypothesis applied to the geometric model and using often the finite volume method. The numerical simulation allows predicting results with a large variation of the problem parameters and boundary conditions that are difficult and sometimes impossible in the practice. On the other hand, the numerical approach has always presented problems, relative to the instationary nature of the flows and the complexity of the variable geometry, which induce a long time of simulation and require computers with high memory capacities. Many works concerned with flows inside cylinders of internal combustion engines have been carried out. Some authors introduced considerable simplifications to the process, among which particularly the assimilation of the valve to a simple disk fixed or moving (Gosman and Tsui,1984; Wakisaka and Shimamoto, 1986; Brandstätter and Johns, 1985; Schapertons and Thiele 1986; Aita and Tabbal, 1991). and the consideration of axisymmetric cylinder with axial valve (Raghay and Hakim, 1997; Giovanni and Karaginnis,1988 ; Mao and Buffat, 1994).Some of these works have not experimental support while others have presented important experimental validations. More recently, the development of the calculation tools permitted improvement in precision and quality of numerical simulations (Chen and Veshagh, 1998; Dillies and Ducamin, 1997; Celik and Yavuz, 2001) based often on the finite volume method especially by means of CFD calculation codes (Payri and Benajes, 2004).

So, our work is essentially about the numerical simula-

lation of aerodynamic and thermal fields in axial plane of axisymmetric cylinder with axial valve and flat piston of internal combustion engine (Figure 1) in order to compare results with others coming from experiments and numerical predictions provided by literature. Our target is to develop and test a numerical methodology based on finite element method by means of powerful calculation code (CASTEM 2000 of CEA) (Gounand ,1997) with tools box offering numerous functions and whose progressive structure allows developing persona-lized procedures. The advantage of finite element method is to permit formulations where fluid is coupled with structure such as study of aerothermic problem coupled with resolution of energy equation in the structure of piston-cylinder.

To take the variability of the domain into account and so the deformed mesh (Haworth and Jansen, 2000; Malcevic and Ghattas, 2002), we have tried to test the arbitrary Lagrangian Eulerian method (ALE) (Souli and Zolesio, 2001). For spatial discretization of fluid domain, the finite elements of the boundaries of the domain coincide constantly with the fluid particles (Lagrangian formulation), even though within domain and in order to manage the great fluid movements we adopt a different rate of deformed mesh and independent of that of fluid. The mesh is deformed with the speed of fluid particles on the moving domain boundaries (piston and valve). The rest of domain is deformed with the speed obtained from an interpolation model between the moving wall speed and the nil speed of fixed wall so as to preserve a good quality of the mesh.

MATHEMATICAL FORMULATION

The average equations describing the flow which is instationary, incompressible and turbulent derived from principles of preservation of mass, momentum, energy and k − ε turbulent entities. These equations are:

Continuity equation:

$$\frac{\partial \rho}{\partial t} + div(\rho \underline{\mathbf{U}}) = 0 \qquad (1)$$

Momentum equation:

$$\frac{\partial \rho.(\underline{\mathbf{U}})}{\partial t} + div(\rho.\underline{\mathbf{U}} * \underline{\mathbf{U}}) = -\nabla P - \frac{2}{3}\nabla((\mu + \mu_t).\nabla u) + \nabla((\mu + \mu_t).(\nabla \underline{\mathbf{U}} + (\nabla \underline{\mathbf{U}})^t))$$

(2)

Where μ_t represents turbulent viscosity given by:

$$\mu_t = C_\mu \rho \frac{k^2}{\varepsilon} \qquad (3)$$

C_μ is a constant, $\underline{\mathbf{U}} * \underline{\mathbf{U}}$ is the matrix ($u_i u_j$).

k-ε equations:

$$\frac{\partial \rho k}{\partial t} + div(\rho.\underline{\mathbf{U}}.k) = div((\mu + \frac{\mu_t}{\sigma_k})\nabla k) + \rho.G - \rho\varepsilon \qquad (4)$$
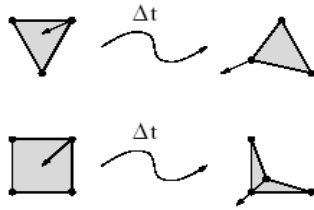
Figure 2. Intake phase configuration

$$\frac{\partial \rho \varepsilon}{\partial t} + div(\rho.\underline{U}.\varepsilon) = div((\mu + \frac{\mu_t}{\sigma_\varepsilon})\nabla \varepsilon) + C_{\varepsilon 1}\rho \frac{\varepsilon}{k}G - C_{\varepsilon 2}\rho \frac{\varepsilon^2}{k} \quad (5)$$

$$G = -\overline{\overset{+}{\underline{U}}*\overset{+}{\underline{U}}} : \nabla \overset{o}{\underline{U}}$$

$$-\rho \overline{\overset{+}{\underline{U}}*\overset{+}{\underline{U}}} = \mu_t(\nabla \overset{o}{\underline{U}} + (\nabla \overset{o}{\underline{U}})^t) - \frac{2}{3}(\overline{\rho}k + \mu_t div \overset{o}{\underline{U}})\underline{\underline{I}} \quad (6)$$

The constants of the model derived from many experiments:

$$C_\mu = 0.09 \; ; \; C_1 = 1.44 \; ; \; C_2 = 1.92 \; ; \sigma_\varepsilon = 1.3 \; ; \; \sigma_k = 0.9$$

Energy equation :

$$\frac{\partial(\rho C_p T)}{\partial t} + div(\rho C_p \underline{U}T) = (\frac{\partial}{\partial t} + \nabla)p + div((\lambda + \lambda_t)\nabla T) \quad (7)$$

Configuration and boundary conditions

Due to the complex chamber geometry of the internal combustion engine which is deeply related to industry, we have chosen in this present work to study an axisymmetric configuration with flat piston and axial valve. This geometry simplification allows a good control of dynamic mesh based on finite element discretization and reduces the time of simulation. The general structure of the internal flow of motor is preserved. The boundary conditions adapted to the chosen configuration are listed below:

$$L1: \; T = T_e \; ; \underline{U}_r = 0$$

$$L2: \; \underline{U}_x = 0 ; \underline{U}_r = 0 ; \frac{\partial T}{\partial n} = 0$$

$$L3: \; \underline{U}_x = V_p \; ; \underline{U}_r = 0 ; \frac{\partial T}{\partial n} = 0$$

$$L4: \; \frac{\partial \underline{U}_x}{\partial n} = 0 ; \underline{U}_r = 0 ; \frac{\partial T}{\partial n} = 0$$

The red frame is composed of the boundaries of the studied domain (L1, L2, L3, and L4) (Figure 2). To express the grip condition, the radial velocity $\underline{U}_r$ and the axial velocity $\underline{U}_x$ of all points that belong to the boundaries take a nil value. At the wall L3 $\underline{U}_x$ has the same velocity of the piston. For the temperature, the Neumann condition is employed, only at the wall L1 we find the Dirichlet condition.

V_p represents the piston speed given by the following equation:

Figure 3. Mean piston speed.

$$V_p(t) = \Omega b \left(\frac{a}{b}\sin(\theta) + \frac{1}{2}\frac{\frac{a^2}{b^2}\sin(2\theta)}{\sqrt{(1 - \frac{a^2}{b^2}\sin^2(\theta))}} \right) \quad (8)$$

$$\theta = \Omega.t$$

We plot the mean piston speed V_p at various locations of the piston as it is described by the previous equation (Figure 3).

Numerical procedure

In fluid mechanics, two descriptions are considered for the motion in a continuum media. The first is the Eulerian description, where we focus attention on a particular volume in space. The volume is fixed and we study the fluid as it passes through it. The description is one in which the fluid is continuously renewed inside the volume; the eulerian description is not the simplest in which the basic equations of fluid motion can be formulated. A convective term is introduced to express the material time derivative in the reference configuration. The convective term gives a nonsymmetrical form of the Galerkin formulation. Since the computational domain is fixed, the Eulerian description has the advantage of preserving the mesh regularity. The second is the Lagrangian description, in which we identify and follow a particular region of fluid. The volume of fluid changes in shape, while the total mass remains constant. In the Lagrangian description, the mesh of the computational domain moves with the particle fluid velocity. The motion of the mesh may lead to an element entanglement; this description is preferred for problems with small motion.

For problems with moving boundaries, it is necessary to have a formulation, which allows the mesh to follow the moving boundaries and preserve the element shape. This has been achieved by the arbitrary Lagrangian-Eulerian (ALE) description. The freedom in moving the mesh offered by the ALE formulation is very attractive. Three domains are defined in this method: the first one is called the spatial domain on which the fluid problem is formulated. Because of

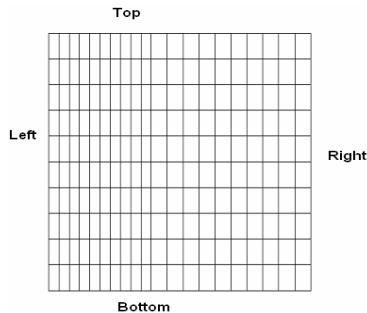**Figure 4.** Examples of degenerated elements.

Figure 5. Moving domain.

moving boundaries this domain is in motion. The second domain, called the material domain, is occupied at time t = 0 by the material particles which occupy the spatial domain at time t. The third domain, called the reference domain, is a fixed domain. The movement of the reference domain is represented by a set of grid points, which may be interpreted as the movement of a finite element mesh. Therefore, in an ALE formulation, the finite element mesh need not adhere to the material or be fixed in space but may be moved arbitrarily relative to the material. A proper ALE formulation should reduce to Lagrangian formulation if we choose to use the same motion for the computational and material meshes. On the other hand, if we choose to fix the computational mesh, an ALE formulation should reduce to Eulerian formulation.

The resolution of equations governing the fluid flow during the intake phase needs a mesh generation and preservation of the number of nodes each step of time.

A finite element method is used to solve the discretized Navier-Stokes equations. To avoid the problem of the domain evolution due to the moving piston the arbitrary Lagrangian Eulerian technique is employed. To pass from a mesh to another one at the next step of time these following constraints are imposed:

- The number and the type of elements mustn't be changed.
- The connections between nodes must be still identical to the previous ones.
- The elements must not degenerate (triangles changing orientation, quadrangles becoming concave …) (Figure 4).

In the ALE description we find two velocities: the first one $\underline{\mathbf{U}}$ represents the velocity of the material particles. The second $\underline{\mathbf{W}}$ is the velocity of the nodes of the reference domain.

If $\underline{\mathbf{W}}$ = 0, we find the Eulerian description. When $\underline{\mathbf{W}} = \underline{\mathbf{U}}$, we return to the Lagrangian description.

The Navier-Stokes equations, applied to a viscous fluid and incompressible, Become in the ALE formulation as indicated below:

Continuity equation:

$$(\frac{\delta}{\delta\, t} + (\underline{\mathbf{U}} - \underline{\mathbf{W}}) \cdot \nabla) \; \rho = - \; \rho \; \nabla .\underline{\mathbf{U}} \tag{9}$$

Momentum equation:

$$\rho \, (\frac{\delta}{\delta\, t} + (\underline{\mathbf{U}} - \underline{\mathbf{W}}) \cdot \nabla) \; \underline{\mathbf{U}} = \rho \; \underline{f}_{v} \; + \nabla \cdot \underline{\underline{\sigma}} \tag{10}$$

The derivative $\dfrac{\delta}{\delta\ t}$ is the variation in unit of time felt by a same point of the reference domain, $\underline{f}_{v}$ is the density of the strength.

We have divided the problem in to three parts: movement of boundary points, movement of internal points and estimate of approximate step of time that prevent the mesh to degenerate. We focus on the domain number four (Figure 5) because it varies during the time. The domain has four boundaries: the bottom boundary represents the piston surface. All points that belong to this surface have a same speed V_p, this speed changes from a step of time to another (Figure 3). The points located on the top boundary are fixed; even though, points at the right and at the left boundaries are linear interpolated between the two speeds zero and V_p.

The movements of internal points of the domain are calculated by resolving the Laplacien equation:

$$\begin{cases} \Delta \underline{\mathbf{W}} = 0 \\ \underline{\mathbf{W}}\big|_{surf} = \underline{\mathbf{W}}^{s} \end{cases} \tag{11}$$

The equation system is solved by means of a program developed with Castem 2000 software.

RESULTS

During the intake phase we consider that the fluid is incompressible. The results are compared to others coming from literature.

Dynamic mesh

The studied domain (Figure 6) of our problem is divided in four domains among which three have a fixed mesh and one has a dynamic mesh since it presents a mobile boundary (the piston). We used this technique to simplify the control of the moving nodes.

The Figures (6a, 6b, 6c, 6d, 6e and 6f) show discretized domain at various crank angle θ = (30°, 60°, 90°, 120°, 150° and 180°) .We see that the adopted method for the mesh movement, arbitrary Lagrangian-Eulerian, has preserved the domain structure, the number and the type of elements. We have not noticed any degeneration. In fact we have used the quadrangular elements for discretization and with the variation of the crank angle the quadrangles do not change the form. The step of time is
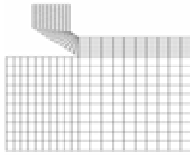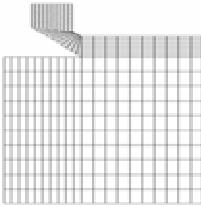
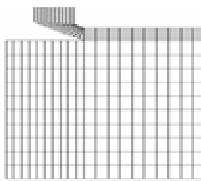**Figure 6a**. Mesh for θ = 30°

Figure 6b. Mesh for θ = 60°

Figure 6c. Mesh for θ = 90°

Figure 6d. Mesh for θ = 120°

Figure 6e. Mesh for θ =150°

taken equal to: PDT=7.10-6 s.

Velocity field and streamlines
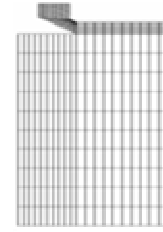
We present the velocity field and the streamlines during
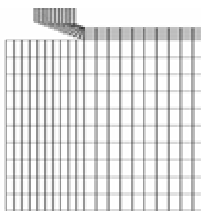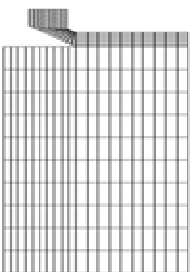
Figure 6f. Mesh for θ =180°

the intake phase. We varied the crank angle from θ equal to 30° to θ equal to 180° with a step of 30°. The control of the velocity distribution inside the combustion chamber improves the quality of the flame and makes an economic fuel mixture. As it is known, the presence of a swirl is preferable in the combustion phenomenon.

The Figures 7a, 7b and 7c prove that the flow structure is swirling presenting a large swirl which fills almost all the combustion chamber. During the variation of the crank angle θ the structure of the large swirl is preserved. The air is drawn by the downward motion of the piston and forms an annular jet. The annular jet expands in the engine cylinder, interacts with the cylinder walls, the piston head and the axial valve. When the air flow reaches the combustion chamber through the valve, it expands, impinges directly on the right cylinder wall and divides in two parts. Part of the flow goes downward along the right cylinder wall and impinges on the piston head. The piston is moving downward and drawing the flow with its face velocity, so that the velocity vectors located a little above the piston head are pointing downward. The second part of the flow, when it impinges the right cylinder wall makes a turn moves up toward the axial valve.

However, we see in Figure 7f that the velocity becomes weak when we approach to θ = 180°.This is due to the evolution of the piston speed which reaches a nil value at the crank angle equal to 180°.

In the Figures 8a, 8b and 8c we note besides the large swirl the formation of other two small swirls: one of them located at the right top corner, the other one at the entry of the cylinder opposite to the valve boundary.

The Figures 7c, 9a and 9b show a good resemblance between results predicted by our numerical code and those predicted on the one hand by Raghay and Hakim and on the other hand by Theodorakakos (1997). In fact, the large middle swirl and the small one at the right top corner exist in the three figures; also the general structure of the moving flow is the same in these different predictions. We draw in the Figure 10 the average axial velocity on the line having a coordinate x = 2.7 cm in different radial coordinates in order to compare with those presented in Figure 11. Figure 11 shows experimental and numerical results done by Raghay and Hakim We notice a good coincidence between the different profiles, this proves another time that our numerical code gives
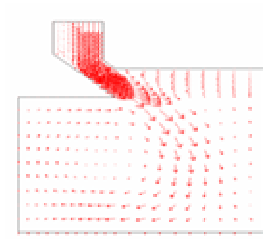
Figure 7a. Velocity field predicted by our numerical code for θ = 30°
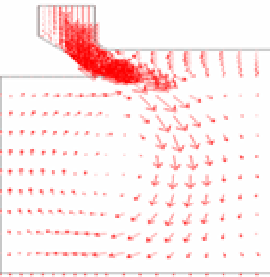
Figure 7b. Velocity field predicted by our numerical code for θ = 60.
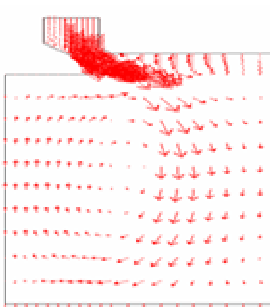
Figure 7c. Velocity field predicted by our numerical code for θ = 90°
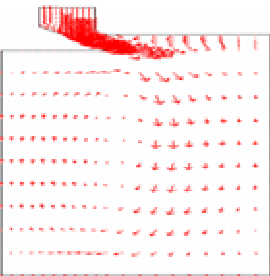
Figure 7d. Velocity field predicted by our numerical code for θ = 120°

satisfied results.

Temperature field
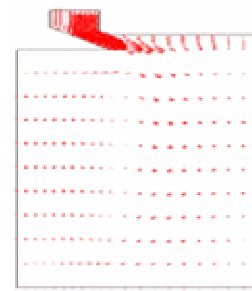
The knowledge of the temperature distribution inside a

Figure 7e. Velocity field predicted by our numerical code for θ = 150°.

Figure 7f. Velocity field predicted by our numerical code for θ = 180°.


```
A -6.13E-02
B -4.80E-02
C -3.47E-02
D -2.14E-02
E -8.09E-03
F  5.22E-03
G  1.85E-02
H  3.18E-02
I  4.51E-02
J  5.85E-02
K  7.18E-02
L  8.51E-02
```
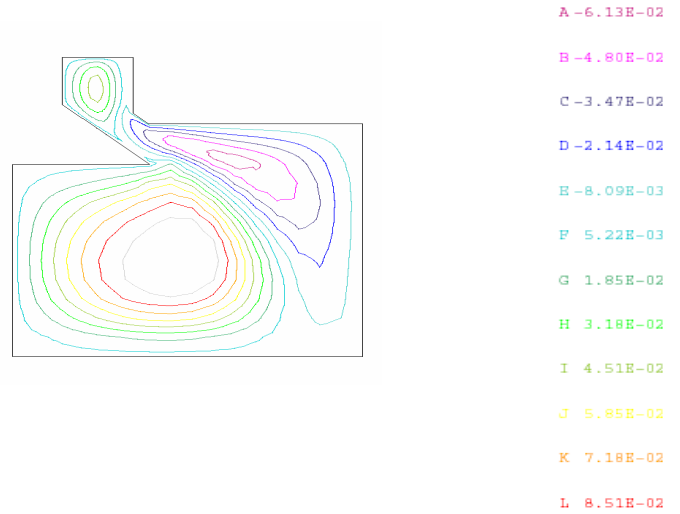
Figure 8a. Streamlines predicted by our numerical code for θ = 30°

combustion chamber of an alternative engine is fundamental. In fact, the good combustion needs a determined temperature which creates flame. As well, the temperature can disrupt the engine functioning since the engine is made of materiel that dilates and as consequence, the dimensions of the different parts which form the engine change.
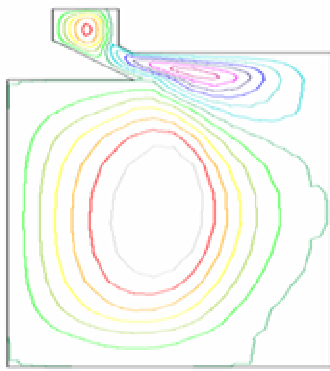
Figure 8b. Streamlines predicted by our numerical code for θ = 90°
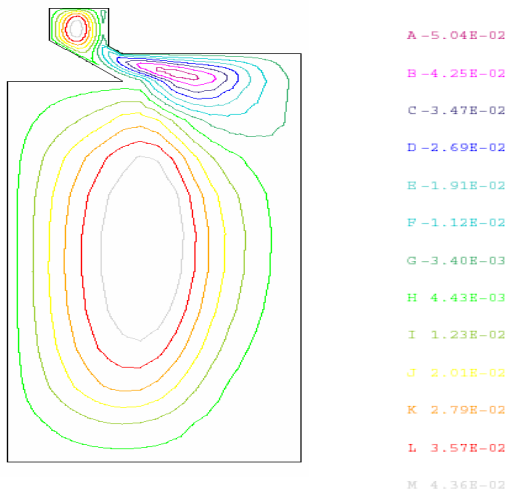
Figure 8c. Streamlines predicted by our numerical code for θ=150°

Figure 9a. Velocity field predicted by Raghay and Hakim for θ = 90°

Turbulent kinetic energy

Various models have been proposed to study the turbulent phenomenon in reacting flow system. The most popular model is the standard k – ε model of Launder and Spalding (1974), the turbulence kinetic energy k and its

Figure 9b. Velocity field predicted by Theodorakakos [26] for θ = 90°
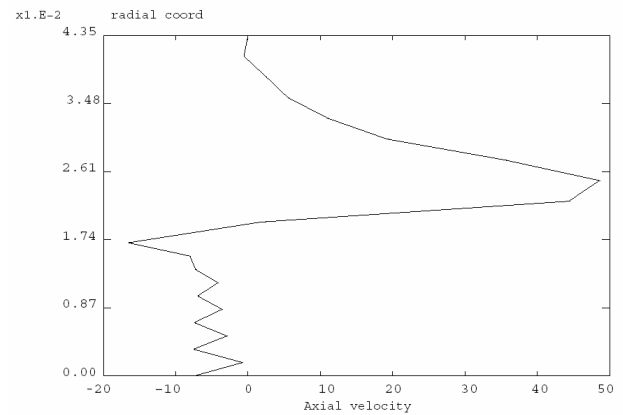
Figure 10. Evolution of the axial velocity at various radial coordinates on the line situated at coordinate x = 2.7 cm predicted by our numerical code.
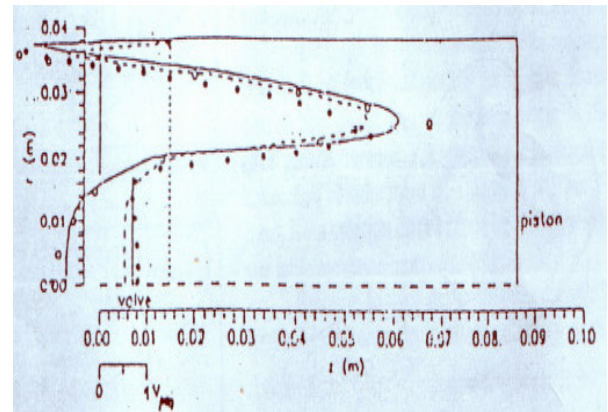
Figure 11. Experimental and numerical evolutions of the axial velocity at various radial coordinates on the line situated at coordinate x = 2.7 cm presented by Raghay and Hakim.

When we discuss the results in Figures 12a, 12b and 12c we conclude that the temperature field presents two
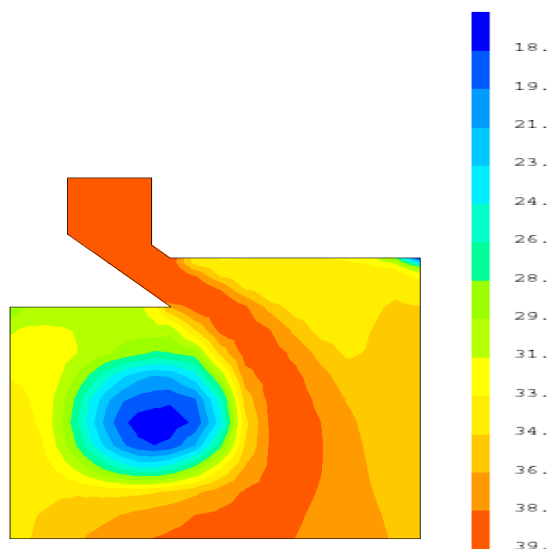
Figure 12a. Temperature field predicted by our numerical code for θ = 30°
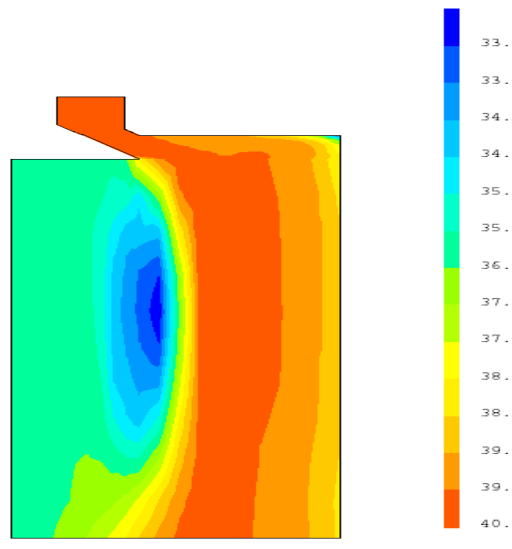
Figure 12c. Temperature field predicted by our numerical code for θ = 150°
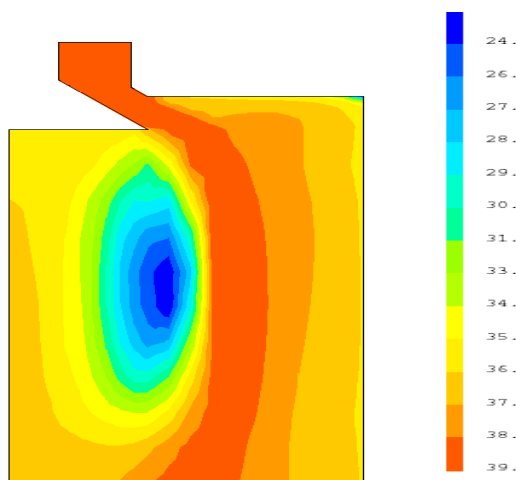
Figure 12b. Temperature field predicted by our numerical code for θ = 90°.

zones: the first one is located from the middle of the large swirl, the blue zone, to the red band whose temperature is Te, the second begin from the last zone to the right boundary of the cylinder. The temperature is minimum at the middle of the swirl and at the right top of the corner and it is maximum in the red band. The temperature increases from the centre of the swirl to the red band then decreases until the right wall of the cylinder. dissipation rate ε are calculated from transport equations in the fully turbulent flow region, and the Reynolds-stress tensor is represented by an eddy viscosity model constructed from k, ε and mean flow field. The turbulent eddy viscosity can be determined from the transport

equation of k and ε. For wall bound flows, wall functions are added to blend the fully turbulent region with the near wall region, because of the predorninance of viscous effects in that region. Used in conjunction with wall functions, the k - ε model is reasonably well behaved, and has been applied to the solution of many practical problems with a good amount of success.

In the Figures 13a →14d we present the distribution of the turbulent kinetic energy K and the dissipation of turbulent kinetic energy ε according to the crank angle θ. We see in the Figures 13a, 13b, 13c and 13d that the turbulent kinetic energy and the dissipation of the turbulent kinetic energy intensify on the right part of the large swirl. This part represents the first domain of the total cylinder domain in which the inlet air expands. K and ε are maximum in the red zone and minimum in the blue zone. In the Figures 14a, 14b, 14c and 14d, we notice that the maximum turbulent kinetic energy and the dissipation of the turbulent kinetic energy change progressively from the right to the left part of the large swirl especially when θ approaches to 180°.

Conclusion

Generally, this study showed that the numerical simu-lations, by means of the adopted model, lead to the identification of the flow structure in the cylinder axial plane during the intake stroke with a precision physically reasonable compared to the results of: Raghay and Hakim, Huang and Chang, Payri and Benajes. It allowed, in particular, emphasizing the process of establishment of different swirling structures in a cylinder with flat piston and axial valve. Although most of similar numerical studies found in literature use the finite volume method,
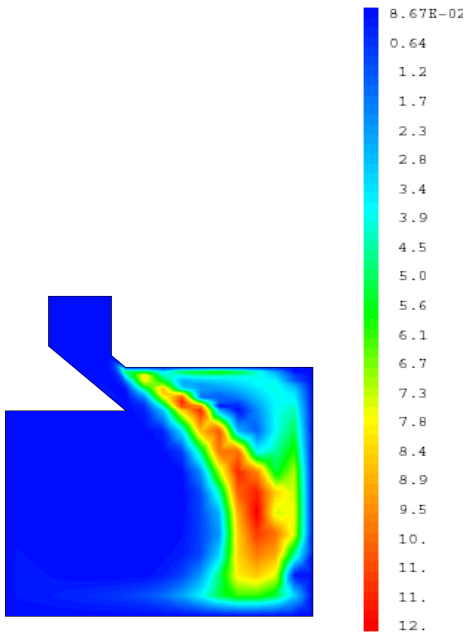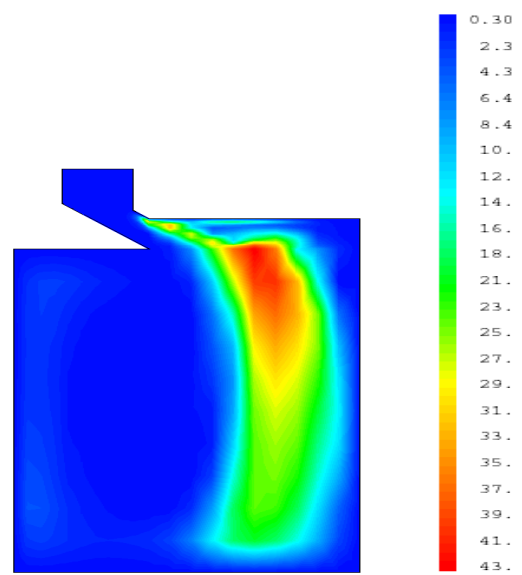
Figure 13a. Turbulent kinetic energy for θ = 30°
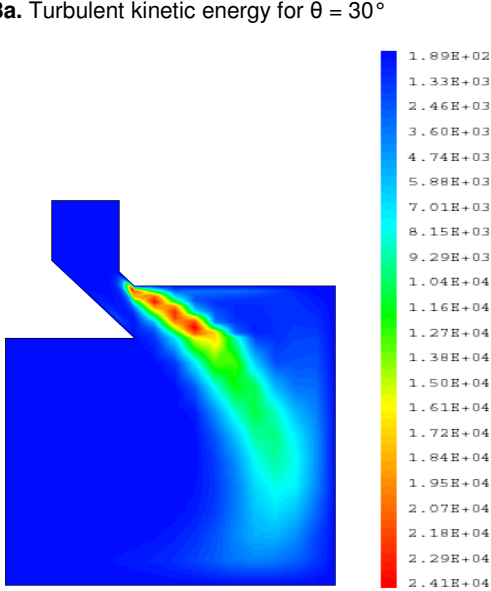

Figure 13c. Turbulent kinetic energy for θ = 90°.

Figure 13b. Dissipation of turbulent kinetic energy for θ = 30°

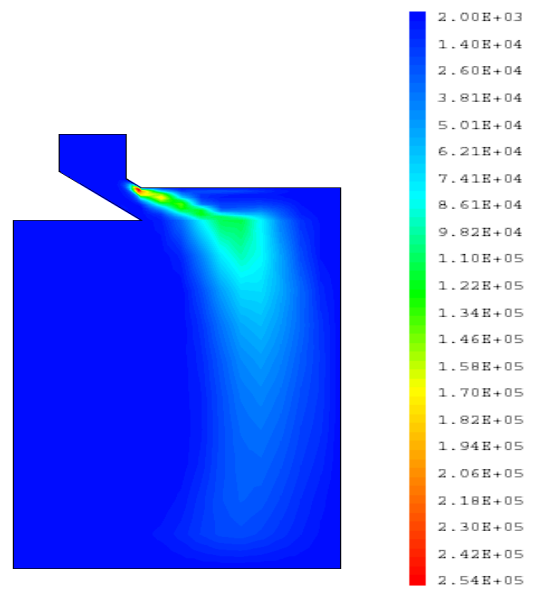**Figure 13d.** Dissipation of turbulent kinetic energy for θ = 90°

this study shows that it is possible to develop a numerical methodology, through a multi-purpose code, based on the finite element method using the Arbitrary Lagrangian Eulerian description, with acceptable simulation time if the size of the problem is relatively limited. The finite element method presents mainly two advantages in comparison to the oldest approach of finite volume method used in the traditional CFD tools. First, the finite elements accept easily complex shapes and geometries. Second, the methodology of the finite element method is based especially on mathematics than physics contrary to the finite volume method. With a same given mesh,

finite element method provides the best solution (minimum error) and gives more large tolerance towards imperfect meshes (important variation in size from element to other).

We have to notice that the quality of the results depends naturally on the mesh fineness but we have to give attention to the step of time to avoid problems of instability and divergence. The advantage of the arbitrary Lagrangian Eulerian method lies in its separate steps which make up the whole proceeding (resolution of Navier_Stokes equations without considering the mesh movement). On the other hand, all the matrix of the sys-
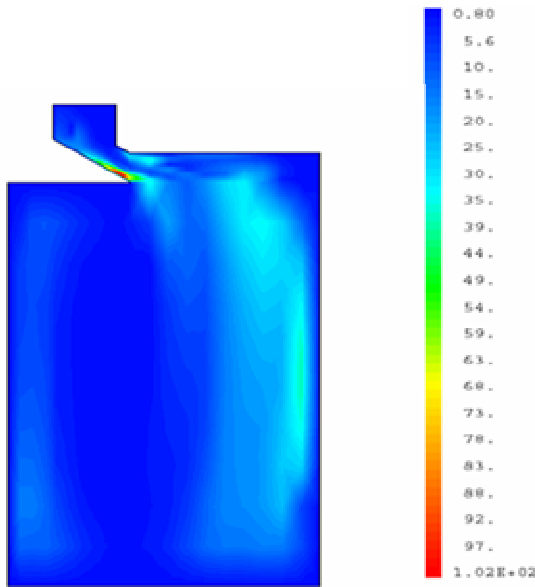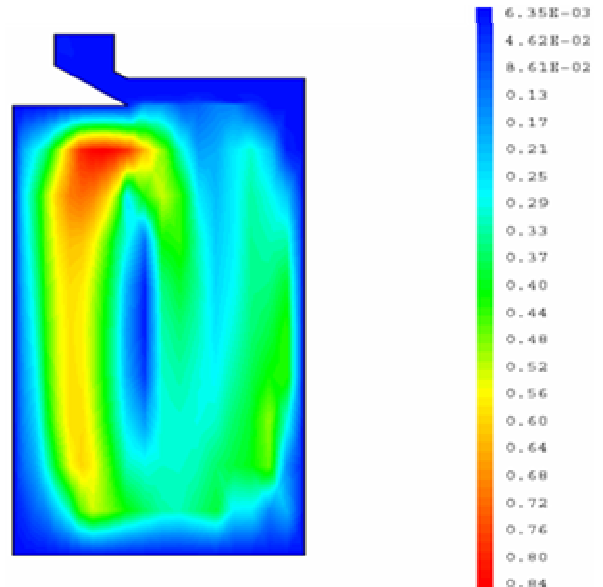
Figure 14a. Turbulent kinetic energy for θ = 120°.

Figure 14c. Turbulent kinetic energy for θ =180°.

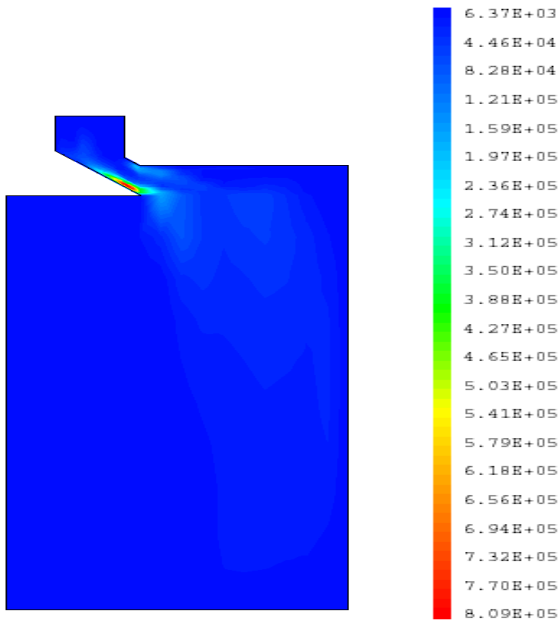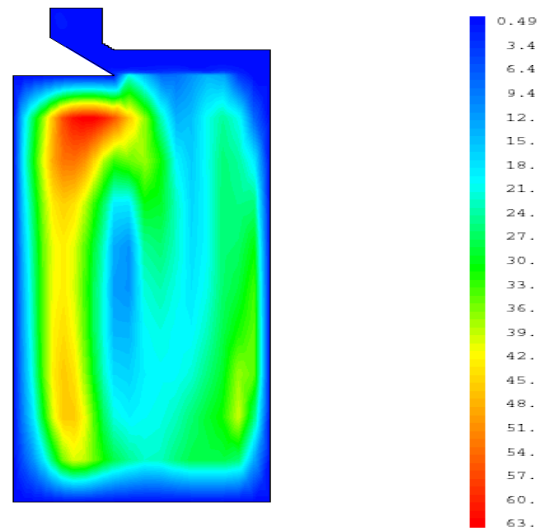**Figure 14b.** Dissipation of turbulent kinetic energy for θ = 120°

Figure 14d. Dissipation of turbulent kinetic energy for θ = 180°.

tem depend on time, so they must be calculated each step of time that increases the time of simulation and the quality of the results (mesh deforming, convergence, stability) is very sensitive to the adopted step of time. The resolution of the energy equation with the same nume- rical methodology and the adopted boundary conditions allow the simulation of the air temperature field at the end of the intake stroke. The knowledge of the temperature field and the pressure distribution allow evaluating the air density at the end of the intake and the rate of filling up of the cylinder.

Finally, the implementation of the ALE description in a program based on the finite element method and going further especially into the research of algorithms more developed concerning the mesh movement and the improvement of programming time, can offer an interest- ing tool for the research and the development in the field of internal aerodynamics of engines.

Notation

a = length of crankshaft (m); b = length of connecting rod (m); C_p = constant pressure specific heat (J.kg^{-1}.K^{-1}); k =

turbulent kinetic energy ($m^2.s^{-2}$); p = pressure (pa); r = radial coordinate (m); R = radius of the combustion chamber (m); S = stroke (m); t = time (s); T = temperature (°K); T_e = inlet temperature (°K); $\underline{U}$ = fluid velocity vector ($m.s^{-1}$); U_x = fluid axial velocity ($m.s^{-1}$);

U_r = fluid radial velocity ($m.s^{-1}$); V_p = mean piston speed ($m.s^{-1}$); $\underline{W}$ = mesh velocity ($m.s^{-1}$); $\underline{W}^s$ = mesh velocity at boundaries ($m.s^{-1}$); x = axial coordinate (mμ =laminar viscosity coefficient ($kg.m^{-1}.s^{-1}$); μ_t = turbulent viscosity coefficient ($kg.m^{-1}.s^{-1}$) λ = thermal conductivity ($w.m^{-1}.K^{-1}$); λ_t = turbulent thermal conductivity ($w.m^{-1}.K^{-1}$); Ω = crankshaft rotational speed ($rd.s^{-1}$); θ = crank angle (degrees); ρ = density ($kg.m^{-3}$); ε = dissipation rate of turbulence ($m^2.s^{-3}$) ;α = seat angle (degrees); $\underline{\underline{\sigma}}$ = viscous stress tensor (N. m^{-2}).

Subscripts: TDC = top dead center; BDC = Bottom dead center.

Superscripts '' = Favre fluctuating quantity; ~ = Favre-averaged quantity
___ = Reynolds-averaged quantity.

REFERENCES

Adrian R (1991). Particle-imaging techniques for experimental fluid mechanics, Ann. Rev. Fluid Mech. 23: 261-304.

Aita S, Tabbal A, Munk G, Monmayeur N, Takenka Y, Aoyagi Y (1991). Numerical simulation of swirling port-valve-cylinder flow in Diesel engine, SAE 910263.

Arcoumanis C, Bicen AF, Vlachos NS, Whitelaw JH (1982). Effects of flow and geometry boundary conditions on fluid motion in a motored IC model engine, Proc Inst. Mech. Eng. 196: 1-10

Arcoumanis C, Bicen AF, Whitelaw JH (1982). Measurement in a motored four stroke reciprocating model engine, J. Fluids Eng. 104: 235

Brandstätter W, Johns RJR, Wigley G (1985). The effect of inlet port geometry on in-cylinder flow structure, SAE 850499

Celik I, Yavuz I, Smirnov A (2001). Large eddy simulations of in-cylinder turbulence for internal combustion engines, a review. Int. J. Eng. Res., 2(2): 119-48.

Chen A, Veshagh A, Wallace S (1998). Intake flow predictions of a transparent DI Diesel Engine, SAE 981020.

Dillies B, Ducamin A, Lebrere L, Neveu F (1997). Direct injection Diesel engine simulation : a combined numerical and experimental approach fro aerodynamics to combustion, SAE 970880,

Ekchian A, Hoult DP (1979). Flow visualization study of the intake process of an internal combustion engine. SAE paper 790095, Warrendale, PA, USA.

Gazeaux J, Thomas DG (2001) Caractérisation du mouvement de rotation de l'air en écoulement stationnaire dans un monocylindre Diesel en fonction des conditions d'admission , Entropie n°., 234 : 13-19.

Giovanni A, Karaginnis F (1988). Caractérisation des grosses structures rotationnelles de l'écoulement dans le cylindre du moteur alternatif par la méthode des tourbillons aléatoires. Entropie n° 139.

Gosman AD, Tsui YY, Watkins AP (1984). Calculation of three dimensional air motion in model engines, SAE 840229,

Gounand S (1997). simulation numérique d'écoulement à surface libre CEA/Saclay, Département de mécanique et de technologie, Service d'études mécaniques et thermiques, Rapport DMT.

Haworth DC, Jansen K (2000). Large-eddy simulation on unstructured deforming meshes: towards reciprocating IC engines, Comput. Fluids 29: 493-524.

Heywood JB (1987). Fluid motion within the cylinder of internal combustion engines, ASME J. Fluids Eng., 109: 3-35.

Hirotimi T, Nagayama I, Kobayashi S, Yamamasu T (1981). Study of induction swirl in a spark ignition engine, SAE paper 810496, Warrendale, PA, USA.

Huang Rf, Huang CW, Yang HS, Lin TW, Hsu WY (2005). Topological flow evolutions in cylinder of motored engine during intake and compression strokes, J. Fluids Struct., 20: 105-127

Kang KY, Reitz RD (1999). Intake flow structure and swirl generation in a four-valve Diesel engine. Spring Technical Conference, ASME, ICE-vol. 32-2. Paper no. 99-ICE-182.

Khalighi B (1991). Study of the intake tumble motion by flow visualization and particle tracking velocimetry, Exp. Fluids 10: 230-236.

Lee J, Farrel PV (1993). Intake valve flow measurements of an IC engine using particle image velocimetry, SAE paper 930480, Warrendale, PA, USA.

Liou T, Saltavicca DA (1985). Cycle resolved LDV measurements in a motored IC engine, ASME J. Fluids Eng., 107, 232-240

Malcevic I, Ghattas O (2002). Dynamic mesh finite element method for Lagrangian computational fluid dynamics, Finite Element Anal. Design 38: 965-982.

Mao Y, Buffat M, Jeandel D (1994). Simulation of the turbulent flow inside the combustion chamber of a reciprocating engine with a finite element method, J. Fluid Eng, p. 116 .

Nadarajah S, Balabani S, Tindal MJ, Yianneskis M (1998). The effect of swirl on the annular flow past an axisymmetric poppet valve, Proc. Inst. Mech. Eng. Part C 212: 473-484

Payri F, Benajes J, Margot X, Gil A (2004). CFD modelling of the in-cylinder flow in direct-injection Diesel engines, Comput. Fluids 33: 995-1021.

Raffer M, Willert CE, Kompenhans J (1998). Particle Image Velocimetry. A Practical Guide. Springer, Berlin.

Raghay S, Hakim A (1997). Simulation numérique d'un écoulement dans un moteur alternatif , Entropie n° 206: 33-42

Rouland E, Floch A, Ahmed A, Dionnet D, Trinite M (1998). Characterization of intake generated tumble flow in 4-valve engine using cross-correlation particle image velocimetry. Proceedings of the Eighth International Symposium on Flow Visualization. 1-15

Schapertons H, Thiele F (1986). Three dimensional computations for flow fields in DI piston bowls , SAE 860464 .

Snauwaert P, Sierens R (1986). Experimental study of the swirl motion in direct injection Diesel engines under steady state flow conditions », SAE 860026

Souli M, Zolesio JP (2001). Arbitrary Lagrangian-Eulerian and free surface methods in fluid mechanics , Comput. Methods Appl. Mech. Eng., 191: 451-466.

Tippelmann G (1977). A new method of investigation of swirl ports, SAE 770404

Valentino G, Kaufman D, Farrel PV (1993). Intake valve flow measurement using PIV, SAE paper 932700, Warrendale, PA, USA.

Wakisaka T, Shimamoto Y, Issihiki Y (1986). Three-dimensional numerical analysis of in- cylinder flows in reciprogating engines, SAE 860464

Yun JE (2002). New evaluation indices for bulk motion of in-cylinder flow trough intake port system in cylinder head, J Automobile Eng. 216: 513- 521.